Chemistry Research Journal, 2024, 9(1):136-146
Available online www.chemrj.org

Research Article

ISSN: 2455-8990
CODEN(USA): CRJHA5

A note on 4-aminoquinoline derivatives as inhibitors of the receptor-interacting protein kinase 2 (RIPK2)

J.S. Gómez-Jeria* and Sabrina Kinney-Garnica

Quantum Pharmacology Unit, Laboratory of Theoretical Chemistry, Department of Chemistry, Faculty of Sciences, University of Chile. Las Palmeras 3425, Santiago CP 7800003, Chile
*E-mail: facien03@gmail.com

Abstract
We have studied the relationships between electronic structure and inhibition of the receptor-interacting protein kinase 2 (RIPK2) in a group of 4-aminoquinoline derivatives. The wave function of all molecules in their protonated form was calculated within the Density Functional Theory at the rmPW1PW91/6-311G(d,p) level after full geometry optimization. We have discovered some electronic requirements in specific atomic centers to enhance inhibitory activity. The associated pharmacophore should provide useful information for the synthesis of new molecules.

Keywords: QSAR, KPG method, Klopman-Peradejordi-Gómez method, electronic structure, 4-aminoquinoline, receptor-interacting protein kinase 2, RIPK2.

1. Introduction

Receptor-interacting serine/threonine-protein kinase 2 (RIPK2) plays an essential role in the immune and inflammatory response system. RIPK2 activity propagates inflammatory signaling through its association with pattern recognition receptors (PRRs) and subsequent TAK1, NF-κB, and MAPK pathway activation. RIPK2 was also shown to play different roles in different cancer types[2-8].

Therefore, RIPK2 represents a new potential therapeutic target for the treatment of diverse conditions, including cancer and inflammatory diseases. Several molecular systems have been synthesized and evaluated for RIPK2 inhibition[9-16].

In this paper we present the results of evaluating the hypothesis stating that the Klopman-Peradejordi-Gómez QSAR method is suitable for finding relationships between electronic structure and RIPK2 inhibitory capacity of a specific group of molecules.

2. Methods, models and calculations[17]

The method

The Klopman-Peradejordi-Gómez (KPG) QSAR method has been presented and explained many times in different papers[18-29]. For this reason we shall present here only the relevant procedures, results and discussion. The application of the KPG method has provided very good results[30-39].

Selection of molecules and biological activities

The selected molecules are a group of 4-aminoquinoline derivatives selected from a recent study[11]. The biological activity analyzed here corresponds to the RIPK2 kinase inhibition. The general formula and inhibitory activity of the compounds selected are displayed, respectively, in Figs. 1 and 2, and Tables 1 and 2.

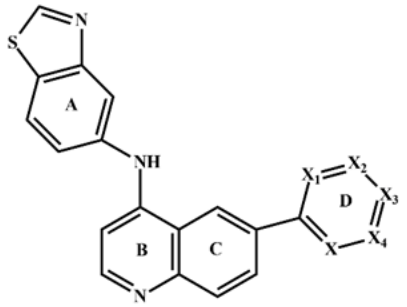

Figure 1: General formulas of group 1 of 4-aminoquinoline derivatives

Table 1: 4-aminoquinoline derivatives and RIPK2 inhibitory activity of group 1.

Molecule	X_1	X_2	X_3	X_4	X	log(RIPK2)
1	C	C	N	C	C	0.71
2	C	N	C	C	C	0.78
3	N	C	C	C	C	0.56
4	C	N	C	N	C	0.18
5	C	C	C	C	C	1.38
6	C	C-CH-CH-NH-C		C	C	1.05
7	C-CH-CH-NH-C		C	C	C	0.97
8	C-CH-N-NH-C		C	C	C	0.57
9	C-CH-CH-NH-C		N	C	C	0.86
10	C	N	C	C-CH-CH-CH-CH-C		1.24
11	C	N	C-CH-CH-CH-CH-C		C	1.62

In molecules 6 to 11 the chains in Table are five-and six-membered rings linking C atoms of ring D.

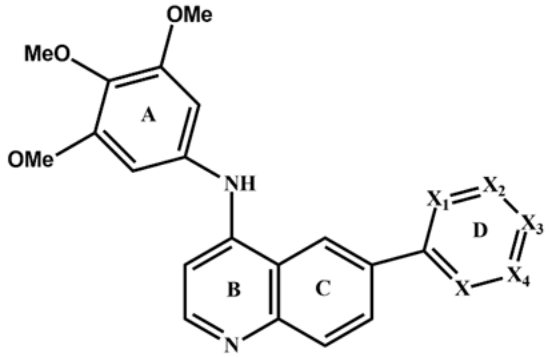

Figure 2: General formulas of group 2 of 4-aminoquinoline derivatives (X=C).

Table 2: 4-aminoquinoline derivatives and RIPK2 inhibitory activity of group 2.

Molecule	X_1	X_2	X_3	X_4	log(RIPK2)
12	C	C	N	C	0.91
13	C	N	C	C	0.38
14	N	C	C	C	1.09
15	C	N	C	N	1.04
16	C-CH-N-NH-C		C	C	0.85

In molecule 16 the chain in Table are five-and six-membered rings linking C atoms of ring D.
Figure 3 shows the histogram of frequencies

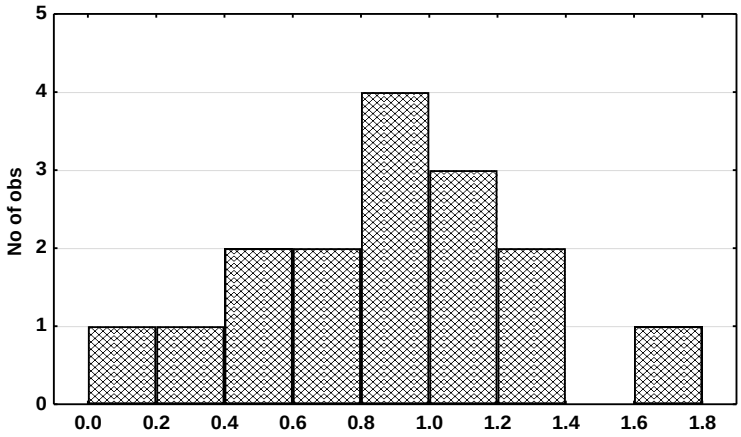

Figure 3: Histogram of frequencies for the experimental data.

Figure 4 shows the Box-Whiskers plot of XXX values with median and quartile values.

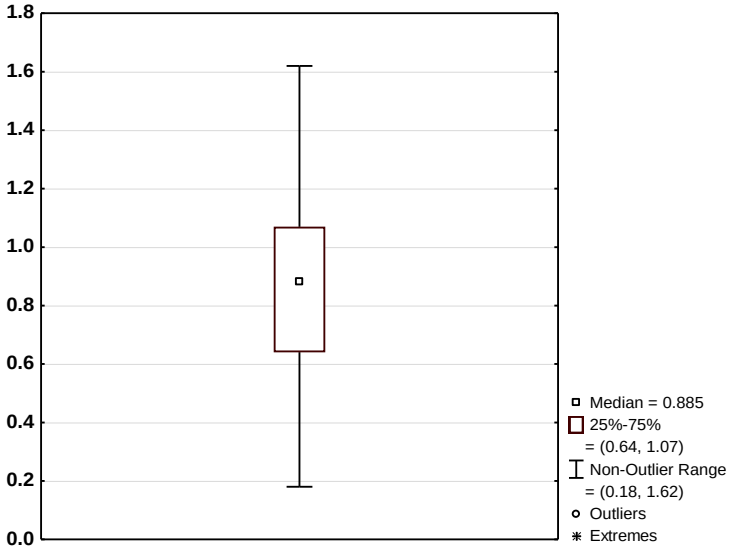

Figure 4: Box-Whiskers plot of experimental values.

3. Calculations[17]

The electronic structure of all molecules was calculated within the Density Functional Theory at the rmPW1PW91/6-311G(d,p) level with full geometry optimization. The Gaussian suite of programs was used[40]. All the information needed to calculate numerical values for the local atomic reactivity indices was obtained from the Gaussian results with the D-Cent-QSAR software[41]. All the electron populations smaller than or equal to 0.01 e were considered as zero. Negative electron populations coming from Mulliken Population Analysis were corrected as usual[42]. We made use of Linear Multiple Regression Analysis (LMRA) techniques to find the best solution. For each case, a matrix containing the dependent variable (the inhibitory activity) and the local atomic reactivity indices of all atoms of a common skeleton as independent variables was built The Statistica software was used for LMRA [43].

The *common skeleton hypothesis* states that there is a definite collection of atoms, common to all molecules analyzed, that accounts for approximately all the inhibitory activity. The action of the substituents consists in

modifying the electronic structure of the common skeleton and influencing the right alignment of the drug throughout the orientational parameters. It is hypothesized that different parts or this common skeleton accounts for almost all the interactions leading to the expression of the inhibitory activity. The common skeleton employed here is shown in Fig. 5. Note that there are other possible common skeletons.

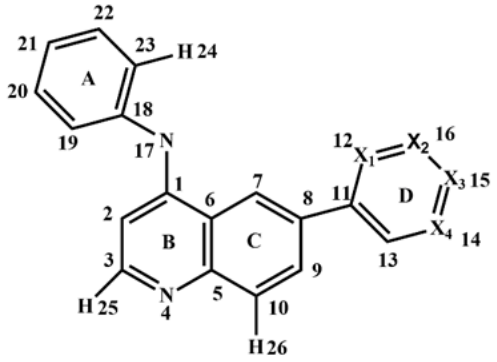

Figure 5. Common skeleton for 4-aminoquinoline derivatives.

4. Results

The best equation obtained was:

$$\log(\text{RIPK2}) = 1.13 - 3.22F_{10}(\text{HOMO}-1)^* + 7.96F_7(\text{LUMO}+2)^* + 1.02F_{11}(\text{HOMO}-1)^* - \\ -0.59F_{22}(\text{LUMO}+2)^* + 1.70S_{22}^{E}(\text{HOMO}-2)^* - 0.75F_{21}(\text{LUMO}+2)^* \quad (1)$$

with n=16, R=0.98, R^2=0.97, adj-R^2=0.95, F(6,9)=47.624 (p<0.00000) and SD=0.08. No outliers were detected, and no residuals fell outside the ±2σ limits. Here, F_{10}(HOMO-1)* is the Fukui index[44] of the second highest occupied *local* molecular orbital (MO) of atom 10 (for *local* molecular orbitals see [28, 29, 45]), F_7(LUMO+2)* is the Fukui index of the third lowest empty local MO of atom 7, F_{11}(HOMO-1)* is the Fukui index of the second highest occupied local MO of atom 11, F_{22}(LUMO+2)* is the Fukui index of the third lowest empty local MO of atom 22, S_{22}^{E}(HOMO-2)* is the electrophilic superdelocalizability of the third highest occupies local MO of atom 22 and F_{21}(LUMO+2)* is the Fukui index of the third lowest empty local MO of atm 21.

Tables 3 and 4 show the beta coefficients, the results of the t-test for significance of coefficients and the matrix of squared correlation coefficients for the variables of Eq. 1.

Table 3: Beta coefficients and t-test for significance of coefficients in Eq. 1.

Variable	Beta	t(9)	p-level
F_{10}(HOMO-1)*	-0.78	-11.54	0.000001
F_7(LUMO+2)*	0.87	10.81	0.000002
F_{11}(HOMO-1)*	0.24	3.29	0.009
F_{22}(LUMO+2)*	-0.28	-3.71	0.005
S_{22}^{E}(HOMO-2)*	0.35	4.77	0.001
F_{21}(LUMO+2)*	-0.29	-4.09	0.003

Table 4: Matrix of squared correlation coefficients for the variables in Eq. 1.

	F_{10}(HOMO1)*	F_7(LUMO+2)*	F_{11}(HOMO1)*	F_{22}(LUMO+2)*	S_{22}^{E}(HOMO-2)*
F_{10}(HOMO-1)*	1.00				
F_7(LUMO+2)*	0.00	1.00			
F_{11}(HOMO-1)*	0.01	0.35	1.00		
F_{22}(LUMO+2)*	0.02	0.09	0.21	1.00	
S_{22}^{E}(HOMO-2)*	0.04	0.02	0.07	0.08	1.00
F_{21}(LUMO+2)*	0.06	0.03	0.00	0.01	0.10

Figure 6 displays the plot of observed *vs.* calculated values.

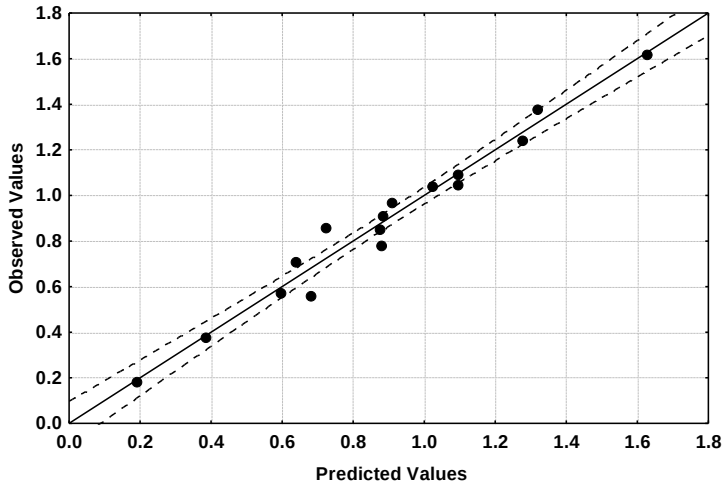

Figure 6: Plot of predicted vs. observed log(RIPK2) values (Eq. 1). Dashed lines denote the 95% confidence interval

The associated statistical parameters of Eq. 1 indicate that this equation is statistically significant and that the variation of the numerical values of a group of six local atomic reactivity indices of atoms constituting the common skeleton explains about 95% of the variation of log(RIPK2). Figure 6, spanning about 1.4 orders of magnitude, shows that there is a good correlation of observed *versus* calculated values.

Figures 7, 8 and 9 show, respectively, the plot of predicted values vs. residuals scores, the plot of residual vs. deleted residuals and the normal probability plot of residuals.

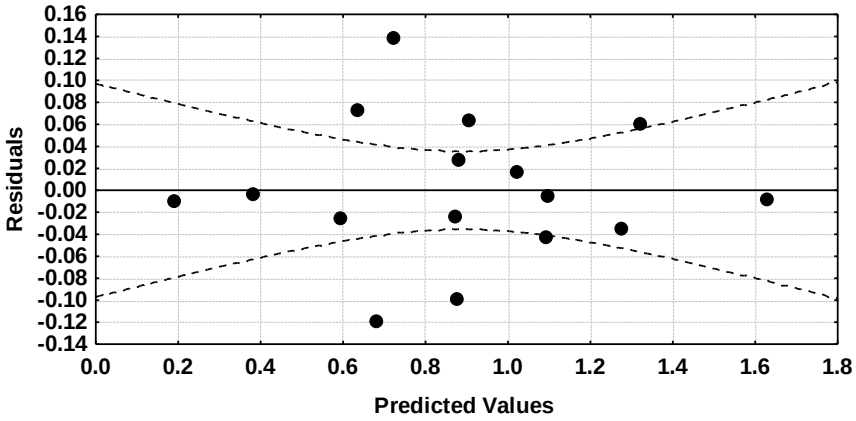

Figure 7: Plot of predicted values vs. residuals scores

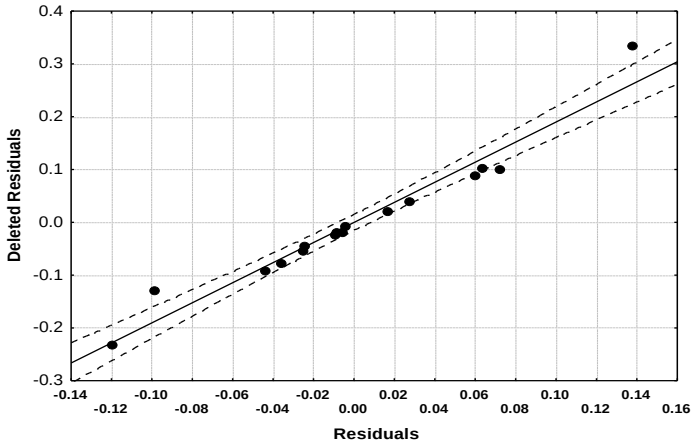

Figure 8: Plot of residuals vs. deleted residuals

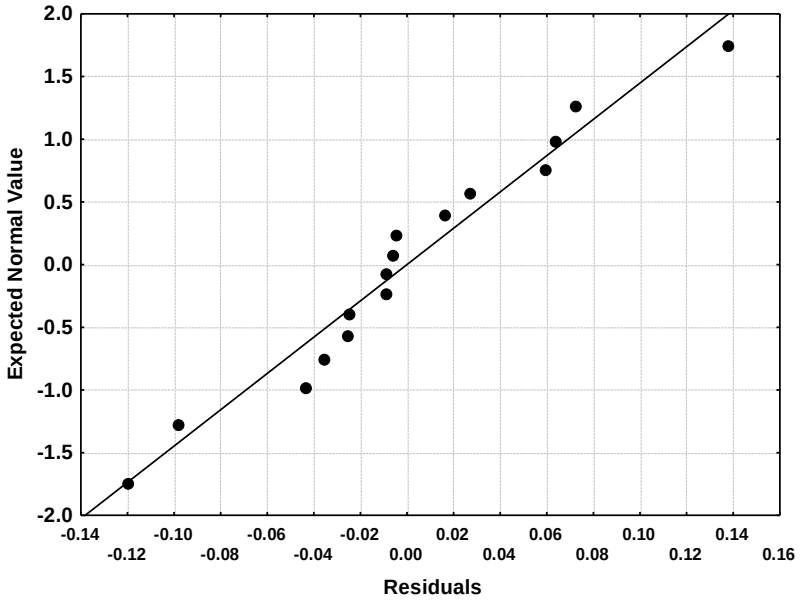

Figure 9: Normal probability plot of residuals

Figures 7 to 9 show that the linear equation 1 is a good approximation to study this biological data and also that the regression coefficients are stable.

Local Molecular Orbitals

Tables 5 and 6 show the local MO structure of atoms 7, 10, 11, 21 and 22 (see Fig. 5). Nomenclature: Molecule (HOMO)/(HOMO-2)*(HOMO-1)*(HOMO)* -(LUMO)*(LUMO+1)* (LUMO+2)*.

Table 5: Local Molecular Orbitals of atoms 7, 10 and 11.

Molecules	Atom 7 (C sp^2)	Atom 10 (C sp^2)	Atom 11 (C sp^2)
1 (92)	89π91π92π-93π96π98π	89π91π92π-93π94π95π	88σ89π91π-93π94π95π
2 (92)	90π91π92π-93π95π97π	90π91π92π-93π94π95π	90π91π92π-93π95π96π
3 (92)	90π91π92π-93π95π96σ	90π91π92π-93π95π97π	87σ90π91π-93π95π96π
4 (92)	89π91π92π-93π97π98π	89π91π92π-93π94π95π	88π89π91π-93π94π95π
5 (92)	90π91π92π-93π95π96π	90π91π92π-93π95π96π	90π91π92π-93π95π97π
6 (102)	99π100π102π-103π105π107π	99π100π102π-103π105π107π	100π101π102π-103π105π106σ
7 (102)	99π100π102π-103π106π107π	99π101π102π-103π105π106π	100π101π102π-103π105π106π
8 (102)	100π101π102π-103π106π107π	98π100π102π-103π105π107π	100π101π102π-103π105π106π
9 (102)	100π101σ102π-103σ106σ107σ	99π100π102π-103π105π106π	100π101π102π-103π105π107π
10 (105)	93π94σ101σ-106π107σ109π	103σ104π105π-106π107π108π	98π101π103π-107π108π109σ
11 (105)	103π104π105π-106π107π110π	103π104π105π-106π107π109π	102π104π105π-106π107π109π
12 (102)	100π101π102π-103π104π106π	100π101π102π-103π104π106π	96π99π101π-103π104π105π
13 (102)	100π101π102π-103π106π107σ	100π101π102π-103π104π106π	99π100π101π-103π104π105σ
14 (102)	100π101π102π-103π104π106π	100π101π102π-103π104π106π	99π100π101π-103π104π105π
15 (102)	100π101π102π-103π105π106π	100π101π102π-103π105π106π	99π100π101π-103π104π105π
16 (112)	110π111π112π-113π114σ115π	110π111π112π-113π114π116π	109σ111π112π-113π114π115π

Table 6: Local Molecular Orbitals of atoms 21 and 22.

Mol. (HOMO)	Atom 21 (C sp^2)	Atom 22 (C sp^2)
1 (92)	90π91π92π-93π94π95π	90π91π92π-93π94π95π
2 (92)	90π91π92π-93π94π95π	90π91π92π-93π94π95π
3 (92)	90π91π92π-93π94π95σ	89π91π92π-94π97π98π
4 (92)	90π91π92π-93π95π97π	90π91π92π-93π94π95π
5 (92)	90π91π92π-93π94π95π	90π91π92π-93π94π95π
6 (102)	100π101π102π-103π104π107π	98π100π102π-104π107π108π
7 (102)	99π101π102π-103π104π106π	95π98π101π-104π106π108σ
8 (102)	100π101π102π-103π104π106π	98π101π102π-104π107π108π
9 (102)	100π101π102π-103π104π105π	100π101π102π-103π104π105π
10 (105)	102π104π105π-106π109π111π	100π102π105σ-109π111π112π
11 (105)	103π104π105π-106π107π108π	101π104π105π-108π110π112π
12 (102)	100π101π102π-103π104π106π	100π101π102π-106π107π108σ
13 (102)	99π101π102π-103π106π107π	99π100π102π-106π107π108π
14 (102)	100π101π102π-103π104π106π	100π101π102π-106π107π108π
15 (102)	100π101π102π-103π105π106π	100π101π102π-107π108π109π
16 (112)	110π111π112π-113π114π116π	110π111π112π-115π116π117π

5. Discussion

Table 3 shows that the importance of variables in Eq. 1 is F_7(LUMO+2)*> F_{10}(HOMO-1)*>> S_{22}^E(HOMO-2)*> F_{21}(LUMO+2)*> F_{22}(LUMO+2)*> F_{11}(HOMO-1)*. A high inhibitory activity is associated with large numerical values for F_{10}(HOMO-1)*, F_{22}(LUMO+2)* and F_{21}(LUMO+2)*, small numerical values for F_7(LUMO+2)* and F_{11}(HOMO-1)*, and large (negative) numerical values for S_{22}^E(HOMO-2)*.

Atom 7 is a sp^2 carbon atom in ring C (Fig. 5). All local frontier molecular orbitals have π nature and coincide with the molecular frontier MOs (Table 5). The only exception is molecule 10: its local HOMO* coincides with an inner occupied MO of the molecule. A high inhibitory activity is associated with small numerical values for F_7(LUMO+2)*. Fukui indices of empty MOs are facing occupied MOs electrophilic superdelocalizabilities[29]. We hold that the condition of a high biological activity and the nature of the mathematical conditions of the indices must be always consistent. The first possibility is to assume that the condition imposed on F_7(LUMO+2)* also holds for F_7(LUMO+1)* and F_7(LUMO)*. This means that atom 7 will become a bad electron acceptor, fact not consistent with the facing of an electron-rich center. The second possibility is to consider that the condition imposed on F_7(LUMO+2)* is only for this index. In this case we could consider that there is a limit on the interaction between empty MOs of atom 7 and occupied MOs of the site. Anyway, the small numerical values for F_7(LUMO+2)* are obtained by making F_7(LUMO+2)*=0. This means that the local $(LUMO+1)_7$* is replaced by an upper empty MO of the molecule. Then, we suggest that atom 7 is interacting with an electron-rich center with at most its two lowest empty local MOs. Note that local HOMO* of molecule 10 coincides with an inner occupied MO. This situation seems to be optimal because the repulsive interactions between occupied MOs from atom 7 and from the site are weakened. The interactions can be at least π-anion and/or π-π ones.

Atom 10 is a sp^2 carbon atom in ring C (Fig. 5). Table 5 shows that all local frontier MOs have a π nature and that all coincide with the molecular frontier MOs. A high inhibitory activity is associated with large numerical values for F_{10}(HOMO-1)*. Fukui indices of occupied MOs are facing nucleophilic superdelocalizabilities of empty MOs[29]. Large numerical values for F_{10}(HOMO-1)* are obtained by maximizing the value of this index: F_{10}(HOMO-1)*=2. In this case the OM is fully localized on atom 7. Then atom 10 is interacting with an electron-deficient center with at least $(HOMO-1)_{10}^*$ and $(HOMO)_{10}^*$. The interactions can be at least π-π and/or π-cation ones.

Atom 11 is a sp^2 carbon atom in ring D (Fig. 5). Table 5 show that all local frontier MOs have a π nature. Local HOMO* coincides with molecular (HOMO), (HOMO-1) or (HOMO-2) depending on the molecule. Local LUMO*

coincides with the molecular (LUMO) or (LUMO+1). A high inhibitory activity is associated with small numerical values for F_{11}(HOMO-1)*. Fukui indices of occupied MOs are facing nucleophilic superdelocalizabilities of empty MOs[29]. The ideal approach is to make F_{11}(HOMO-1)*=0. This means that the actual $(HOMO-1)_{11}^{*}$ will be replaced by another molecular MO having a larger ionization potential. This suggests that atom 11 is interacting with an electron-deficient site only through $(HOMO)_{11}^{*}$. We speculate that inner occupied MOs can be engaged in a repulsive interactions with occupied MOs of the site. The interactions can be at least π-anion and/or π-π ones.

Atom 21 is a sp^2 carbon atom in ring A (Fig. 5). Table 6 shows that all local frontier MOs have a π nature and that all coincide with the molecule's frontier MOs. A high inhibitory activity is associated with large numerical values for F_{21}(LUMO+2)*. Fukui indices of empty MOs are facing occupied MOs electrophilic superdelocalizabilities[29]. The ideal situation is to maximize the value of this reactivity index such as F_{21}(LUMO+2)*=0. In this case this MO will be fully localized on atom 21. We suggest that atom 21 is interacting with an electron-rich center through its first three lowest empty MOs. The interactions can be at least π-π and/or π-cation ones.

Atom 22 is a sp^2 carbon atom in ring D (Fig. 5). Table 6 shows that all local frontier MOs have a π nature. Local HOMO* coincides with the molecular HOMO, and only in one case with the molecular (HOMO-1). Local LUMO* coincides with different molecular empty MOs depending on the molecule (from (LUMO) to (LUMO+4)). A high inhibitory activity is associated with large numerical values for F_{22}(LUMO+2)* and with large (negative) numerical values for S_{22}^{E}(HOMO-2)*. Note that Fukui indices of empty MOs are facing occupied MOs electrophilic superdelocalizabilities[29] and that electrophilic superdelocalizabilities of occupied MOs are facing Fukui indices of empty MOs[29]. This two apparent contradictory constraints can be solved by suggesting that atom 22 is interacting with two sites at the same time ones. Large numerical values for F_{22}(LUMO+2)* are obtained by making F_{22}(LUMO+2)*2. This suggests that atom 22 is interacting with an electron-rich center through its three lowest empty MOs. In this case the interactions can be at least π-π and/or π-anion ones. Large (negative) numerical values for S_{22}^{E}(HOMO-2)* are obtained by shifting the $(HOMO-2)_{22}^{*}$ energy toward zero, making the three highest occupied MOs more reactive. This suggests an interaction of atom 22 with an electron-deficient site. In this case the interactions can be at least π-π and/or π-cation ones.

All the suggestions are displayed in the partial 2D pharmacophore of Fig. 10.

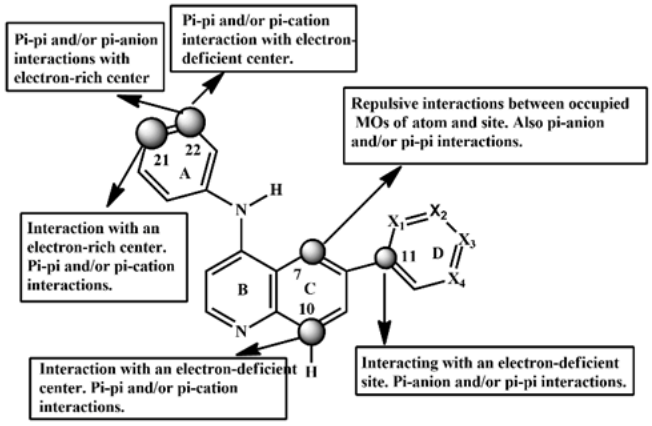

Figure 10: Partial 2D pharmacophore for RIPK2 inhibition.

It should be noted that in this case, as in others that we have reported, the dataset for the LMRA has been created with the following hypothesis about the orientation of the D ring. In all molecules that have an N atom that can be positioned as X1, this has been done. Note that the article from which the experimental data were obtained only presents drawings made by the authors, some of which could be misleading on this subject. This can be seen by comparing the common skeleton with the drawings just mentioned[11]. Obviously, it is possible to fabricate other assemblies with various orientations of the D-ring and conduct several different MRLs, but this is only done if the first hypothesis does not produce statistically significant results. The recommendation is to synthesize compounds in which positions 2 and 6, and 3 and 5 of rings similar to D are replaced by the same atoms.

In summary, we have found a statistically significant relationship between the inhibitory activity of these compounds and a set of local atomic reactivity indices, which should allow us to obtain compounds with greater inhibitory capacity.

References

[1]. All papers of J.S.G.-J. can be found in https://www.researchgate.net/profile/Juan-Sebastian_Gomez-Jeria.
[2]. Zhao, W.; Leng, R.-X.; Ye, D.-Q. RIPK2 as a promising druggable target for autoimmune diseases. International Immunopharmacology 2023, 118, 110128.
[3]. You, J.; Wang, Y.; Chen, H.; Jin, F. RIPK2: a promising target for cancer treatment. Frontiers in Pharmacology 2023, 14, 1192970.
[4]. Tian, E.; Zhou, C.; Quan, S.; Su, C.; Zhang, G.; Yu, Q.; Li, J.; Zhang, J. RIPK2 inhibitors for disease therapy: Current status and perspectives. European Journal of Medicinal Chemistry 2023, 115683.
[5]. Rivoal, M.; Dubuquoy, L.; Millet, R.; Leleu-Chavain, N. Receptor Interacting Ser/Thr-Protein Kinase 2 as a New Therapeutic Target. Journal of Medicinal Chemistry 2023, 66, 14391-14410.
[6]. Pham, A.-T.; Ghilardi, A. F.; Sun, L. Recent advances in the development of RIPK2 modulators for the treatment of inflammatory diseases. Frontiers in Pharmacology 2023, 14, 1127722.
[7]. Honjo, H.; Watanabe, T.; Kamata, K.; Minaga, K.; Kudo, M. RIPK2 as a new therapeutic target in inflammatory bowel diseases. Frontiers in Pharmacology 2021, 12, 650403.
[8]. Tigno-Aranjuez, J. T.; Benderitter, P.; Rombouts, F.; Deroose, F.; Bai, X.; Mattioli, B.; Cominelli, F.; Pizarro, T. T.; Hoflack, J.; Abbott, D. W. In vivo inhibition of RIPK2 kinase alleviates inflammatory disease. Journal of Biological Chemistry 2014, 289, 29651-29664.
[9]. Misehe, M.; Šála, M.; Matoušová, M.; Hercík, K.; Kocek, H.; Chalupská, D.; Chaloupecká, E.; Hájek, M.; Boura, E.; Mertlíková-Kaiserová, H. Design, synthesis and evaluation of novel thieno [2, 3d] pyrimidine derivatives as potent and specific RIPK2 inhibitors. Bioorganic Medicinal Chemistry Letters 2024, 97, 129567.
[10]. Lai, Y.; Wang, X.; Sun, X.; Wu, S.; Chen, X.; Yang, C.; Zhang, W.; Yu, X.; Tong, Y.; Ma, F. Discovery of a novel RIPK2 inhibitor for the treatment of inflammatory bowel disease. Biochemical Pharmacology 2023, 115647.
[11]. Fan, T.; Ji, Y.; Chen, D.; Peng, X.; Ai, J.; Xiong, B. Design, synthesis and biological evaluation of 4-aminoquinoline derivatives as receptor-interacting protein kinase 2 (RIPK2) inhibitors. Journal of Enzyme Inhibition and Medicinal Chemistry 2023, 38, 282-293.
[12]. Yuan, X.; Chen, Y.; Tang, M.; Wei, Y.; Shi, M.; Yang, Y.; Zhou, Y.; Yang, T.; Liu, J.; Liu, K. Discovery of potent and selective receptor-interacting serine/threonine protein kinase 2 (RIPK2) inhibitors for the treatment of inflammatory bowel diseases (IBDs). Journal of Medicinal Chemistry 2022, 65, 9312-9327.
[13]. Wu, S.; Xu, L.; Wang, X.; Yang, Q.; Wang, J.; He, S.; Zhang, X. Design, synthesis, and structure-activity relationship of novel RIPK2 inhibitors. Bioorganic Medicinal Chemistry Letters 2022, 75, 128968.
[14]. Nikhar, S.; Siokas, I.; Schlicher, L.; Lee, S.; Gyrd-Hansen, M.; Degterev, A.; Cuny, G. D. Design of pyrido [2, 3-d] pyrimidin-7-one inhibitors of receptor interacting protein kinase-2 (RIPK2) and nucleotide-binding oligomerization domain (NOD) cell signaling. European journal of medicinal chemistry 2021, 215, 113252.
[15]. Martens, S.; Hofmans, S.; Declercq, W.; Augustyns, K.; Vandenabeele, P. Inhibitors targeting RIPK1/RIPK3: old and new drugs. Trends in pharmacological sciences 2020, 41, 209-224.
[16]. He, X.; Da Ros, S.; Nelson, J.; Zhu, X.; Jiang, T.; Okram, B.; Jiang, S.; Michellys, P.-Y.; Iskandar, M.; Espinola, S. Identification of potent and selective RIPK2 inhibitors for the treatment of inflammatory diseases. ACS medicinal chemistry letters 2017, 8, 1048-1053.
[17]. The results presented here are obtained from what is now a routinary procedure. For this reason, all papers have a similar general structure. This model contains standard phrases for the presentation of the methods, calculations and results because they do not need to be rewritten repeatedly and because the number of

possible variations to use is finite. See: Hall, S., Moskovitz, C., and Pemberton, M. 2021. Understanding Text Recycling: A Guide for Researchers. Text Recycling Research Project. Online at textrecycling.org. In.

[18]. Hudson, R. F.; Klopman, G. A general perturbation treatment of chemical reactivity. Tetrahedron Letters 1967, 8, 1103-1108.

[19]. Klopman, G.; Hudson, R. F. Polyelectronic perturbation treatment of chemical reactivity. Theoretica chimica acta 1967, 8, 165-174.

[20]. Klopman, G. Chemical reactivity and the concept of charge- and frontier-controlled reactions. Journal of the American Chemical Society 1968, 90, 223-234.

[21]. Peradejordi, F.; Martin, A. N.; Cammarata, A. Quantum chemical approach to structure-activity relationships of tetracycline antibiotics. Journal of Pharmaceutical Sciences 1971, 60, 576-582.

[22]. Gómez Jeria, J. S. La Pharmacologie Quantique. Bollettino Chimico Farmaceutico 1982, 121, 619-625.

[23]. Gómez-Jeria, J. S. On some problems in quantum pharmacology I. The partition functions. International Journal of Quantum Chemistry 1983, 23, 1969-1972.

[24]. Gómez-Jeria, J. S. The use of competitive ligand binding results in QSAR studies. Il Farmaco; edizione scientifica 1985, 40, 299-302.

[25]. Gómez-Jeria, J. S. Modeling the Drug-Receptor Interaction in Quantum Pharmacology. In Molecules in Physics, Chemistry, and Biology, Maruani, J., Ed. Springer Netherlands: 1989; Vol. 4, pp 215-231.

[26]. Gómez-Jeria, J. S.; Ojeda-Vergara, M. Parametrization of the orientational effects in the drug-receptor interaction. Journal of the Chilean Chemical Society 2003, 48, 119-124.

[27]. Gómez-Jeria, J. S. Elements of Molecular Electronic Pharmacology (in Spanish). 1st ed.; Ediciones Sokar: Santiago de Chile, 2013; p 104.

[28]. Gómez-Jeria, J. S. A New Set of Local Reactivity Indices within the Hartree-Fock-Roothaan and Density Functional Theory Frameworks. Canadian Chemical Transactions 2013, 1, 25-55.

[29]. Gómez-Jeria, J. S. A Note on Local Molecular Orbitals and Non-linear terms in the Klopman-Peradejordi-Gómez QSAR method. Chemistry Research Journal 2024, 9, 50-57.

[30]. Gómez-Jeria, J. S. On the relationship between electronic structure and herbicidal activity of biphenyl ether derivatives having a five-membered heterocycle. Chemistry Research Journal 2023.

[31]. Gómez-Jeria, J. S.; Soloaga Ardiles, C. E. A Density Functional Theory inquiry of the relationships between electronic structure and anticonvulsant activity in a series of 2,5-disubstituted thiadiazoles. Chemistry Research Journal 2022, 7, 55-68.

[32]. Gómez-Jeria, J. S.; Robles-Navarro, A.; Jaramillo-Hormazábal, I. A DFT analysis of the relationships between electronic structure and activity at D2, 5-HT1A and 5-HT2A receptors in a series of Triazolopyridinone derivatives. Chemistry Research Journal 2022, 7, 6-28.

[33]. Gómez-Jeria, J. S.; Olarte-Lezcano, L. On the relationships between electronic structure and 5-HT2A, 5-HT2C and D2 receptor affinities in a group of 2-aryl tryptamines. A DFT study. Chemistry Research Journal 2022, 7, 14-35.

[34]. Gómez-Jeria, J. S.; Ibertti-Arancibia, A.; Olarte-Lezcano, L. A theoretical study of the relationships between electronic structure of 2-aryladenine derivatives and percentage of inhibition of radioligand binding in human A2A and A2B adenosine receptors. Chemistry Research Journal 2022, 7, 1-18.

[35]. Gómez-Jeria, J. S.; Silva-Monroy, S. A quantum-chemical analysis of the relationships between electronic structure and inhibition of SARS-CoV-2 virus by a group of cyclic sulfonamide derivatives. Chemistry Research Journal 2021, 6, 54-70.

[36]. Gómez-Jeria, J. S.; Robles-Navarro, A.; Soza-Cornejo, C. A note on the relationships between electronic structure and serotonin 5-HT1A receptor binding affinity in a series of 4-butyl-arylpiperazine-3-(1H-indol-3-yl)pyrrolidine-2,5-dione derivatives. Chemistry Research Journal 2021, 6, 76-88.

[37]. Gómez-Jeria, J. S.; Robles-Navarro, A.; Soto-Martínez, V. Quantum Chemical Analysis of the relationships between electronic structure and dopamine D1 and D5 receptor binding affinities in a series of 1-phenylbenzazepines. Chemistry Research Journal 2021, 6, 128-144.

[38]. Gómez-Jeria, J. S.; Ibertti-Arancibia, A. A DFT study of the relationships between electronic structure and dopamine D1 and D2 receptor affinity of a group of (S)-enantiomers of 11-(1,6-dimethyl-1,2,3,6-tetrahydropyridin-4-yl)-5H-dibenzo[b,e][1,4]diazepines. Chemistry Research Journal 2021, 6, 116-131.

[39]. Gómez-Jeria, J. S.; Crisóstomo-Cáceres, S. R.; Robles-Navarro, A. On the compatibility between formal QSAR results and docking results: the relationship between electronic structure and H5N1 (A/goose/Guangdong/SH7/2013) neuraminidase inhibition by some Tamiflu derivatives as an example. Chemistry Research Journal 2021, 6, 46-59.

[40]. Frisch, M. J.; Trucks, G. W.; Schlegel, H. B.; Scuseria, G. E.; Robb, M. A.; Cheeseman, J. R.; Scalmani, G.; Barone, V.; Mennucci, B.; Petersson, G. A.; Nakatsuji, H.; Caricato, M.; Montgomery, J., J.A. Gaussian 09, Revision A.01, Gaussian Inc.: Wallingford CT, 2009.

[41]. Gómez-Jeria, J. S. D-Cent-QSAR: A program to generate Local Atomic Reactivity Indices from Gaussian 09 log files, v. 2.0; Santiago, Chile, 2019.

[42]. Gómez-Jeria, J. S. An empirical way to correct some drawbacks of Mulliken Population Analysis (Erratum in: J. Chil. Chem. Soc., 55, 4, IX, 2010). Journal of the Chilean Chemical Society 2009, 54, 482-485.

[43]. Statsoft. Statistica v. 8.0, 2300 East 14 th St. Tulsa, OK 74104, USA, 1984-2007.

[44]. Fukui, K.; Fujimoto, H. Frontier orbitals and reaction paths: selected papers of Kenichi Fukui. World Scientific: Singapore; River Edge, N.J., 1997; p xvii, 543 p.

[45]. Gómez-Jeria, J. S.; Kpotin, G. Some Remarks on The Interpretation of The Local Atomic Reactivity Indices Within the Klopman-Peradejordi-Gómez (KPG) Method. I. Theoretical Analysis. Research Journal of Pharmaceutical, Biological and Chemical Sciences 2018, 9, 550-561.